Supporting Information

A lightweight 3D Cellular MXene Film for Superior Energy Storage and Electromagnetic Interference Shielding

Zhimin Fan,[a,b] Huaqing He,[b] Jianxin Yu,[c] Li Liu,[b] Yuyan Liu,[b] and Zhimin Xie[d,*]

[a]School of Materials Science and Engineering, Harbin Institute of Technology, Harbin 150001, China
[b]MIIT Key Laboratory of Critical Materials Technology for New Energy Conversion and Storage, School of Chemistry and Chemical Engineering, Harbin Institute of Technology, Harbin 150001, China
[c]Center of Analysis and Measurement, Harbin Institute of Technology, Harbin 150001, China
[d]National Key Laboratory of Science and Technology on Advanced Composites in Special Environments
Harbin Institute of Technology
Harbin 150080, P. R. China

Corresponding author
E-mail addresses: xiezhm@hit.edu.cn

1. Experimental Procedures

Synthesis of $Ti_3C_2T_x$ MXene dispersion. $Ti_3C_2T_x$ MXene was synthesized through etching the parent Ti_3AlC_2 MAX with HCl/LiF mixture to selectively remove Al layers. Typically, 3.2 g of LiF (Aladin) and 40 mL of 9 M HCl (Sinopharm Chemical Reagent Company) were mixed well under magnetic stirring in a polytetrafluoroethylene beaker. Afterward, Ti_3AlC_2 powder (2 g) was slowly added to prevent overheating, and continuously stirred for 24 h at 35℃. The obtained product was then washed and centrifuged repeatedly with deionized water until the pH of supernatant was close to 6. Subsequently, the precipitate was diluted to 200 mL with deionized water and then bath sonicated in an ice bath for 10 min. Finally, the solution was centrifuged at 3500 rpm for 10 min to collect the $Ti_3C_2T_x$ MXene dispersion (5 mg mL^{-1}).

Preparation of 3D cellular MXene film. The MXene microgel dispersion was prepared by using KCl-induced flocculation of MXene dispersion colloid, in which different degrees of MXene microgel were obtained by changing the amount of KCl (0.1, 0.2, 0.5, 1.0, and 2.0 g). Then the MXene microgel dispersion was vacuum filtered through a cellulose membrane (0.45 μm pore size). The vacuum was disconnected once no obvious residual dispersion on the filter membrane. After that, both the MXene hydrogel film and the filter membrane were vertically immersed into liquid nitrogen bath to fast freeze for 10 minutes. Then, this film was vacuum freeze-dried at −65 ℃ (25 Pa) for 24 h, and the acquired 3D cellular MXene film will automatically detach from the filter membrane on the way of freeze-drying. According to the amount of KCl added, the samples were named 3D $CMX_{0.1}$, 3D $CMX_{0.2}$, 3D $CMX_{0.5}$, 3D $CMX_{1.0}$ and 3D $CMX_{2.0}$, respectively. The preparation process of the porous MXene film (PMX) is the same as that of the 3D cellular MXene film except for the direct use of MXene dispersion. As a comparison, the slow freezing of the sample was to freeze for 24 h in the freezing mode of an ordinary household refrigerator; the other steps were similar to the

current method of 3D cellular MXene film. Note that the mass loading of all samples used for the electrochemical performance testing is 1.2 mg cm^{-2}.

Characterization methods. The morphology and microstructure of the prepared samples were observed using a transmission electron microscopy (Tecnai G2 F30, FEI), High-angle-annular-dark-field scanning transmission electron microscopy (HAADF-STEM, Talos F200x, FEI) and scanning electron microscope (SUPRA 55 SAPPHIRE). The atomic force microscopy (AFM) image of MXene nanosheet was acquired in a contact and tapping modes using a Bruker Dimension Fastscan. X-ray diffraction (XRD) measurements were performed on an X-ray diffractometer (D8 Advance, Bruker) with Cu Ka radiation. The electrical conductivity of the prepared samples was measured using an ST2258 (Suzhou jingge Electronic Co., Ltd) four-prob tester. The mechanical properties of the MXene film and 3D celluar MXene film were measured by a conventional electronic tensile machinel using a loading rate of 0.2 mm/min.

Electrochemical measurements. The electrochemical performance measurements of the obtained samples were tested in the 3 M H_2SO_4 aqueous electrolyte on a CHI 760D workstation (Shanghai Chenhua) using a three-electrode configuration, in which the Pt foil, Ag/AgCl and films were used as the counter, reference and working electrodes, respectively. The electrochemical impedance spectroscopy (EIS) was tested at open circuit potential of 5 mV within a frequency range from 10^{-2} HZ to 10^{5} HZ. The gravimetric capacitance (C_{wt}, F g^{-1}) was estimated by the following formulas:

$$C_{wt} = \frac{1}{\Delta V m v}\int i dV \tag{1}$$

Where i is the current density, v is the potential scan rate, m (g) is the mass of electrode, V is the potential windows. Cycling stability measurement was performed by repeating the cyclic voltammetry at 100 mV s^{-1} for 10000 cycles.

Electromagnetic interference (EMI) measurements. EMI shielding performance was tested by An Agilent N5234A vector network analyzer (Keysight Technologies) in X-band frequency range (8.2−12.4 GHz). During the test, the film samples were sandwiched between the waveguide sample holders. The EMI SE was calculated from the scattering parameters (S_{11} and S_{21}) estimated based on the equations:

$$R = |S_{11}|^2 \tag{2}$$

$$T = |S_{21}|^2 \tag{3}$$

$$T + A + R = 1 \tag{4}$$

$$\mathrm{SE_{Total}\ (dB)} = -10 \log \mathrm{T} \tag{5}$$

$$\mathrm{SE_R\ (dB)} = \mathrm{SE_{Total}} - \mathrm{SE_R} \tag{6}$$

Where R, T and A are the reflection, transmission and absorption coefficients, respectively. SE_{Total}, SE_R and SE_A are the total, reflective and absorptive EMI SE, respectively.

2. Supplementary Results

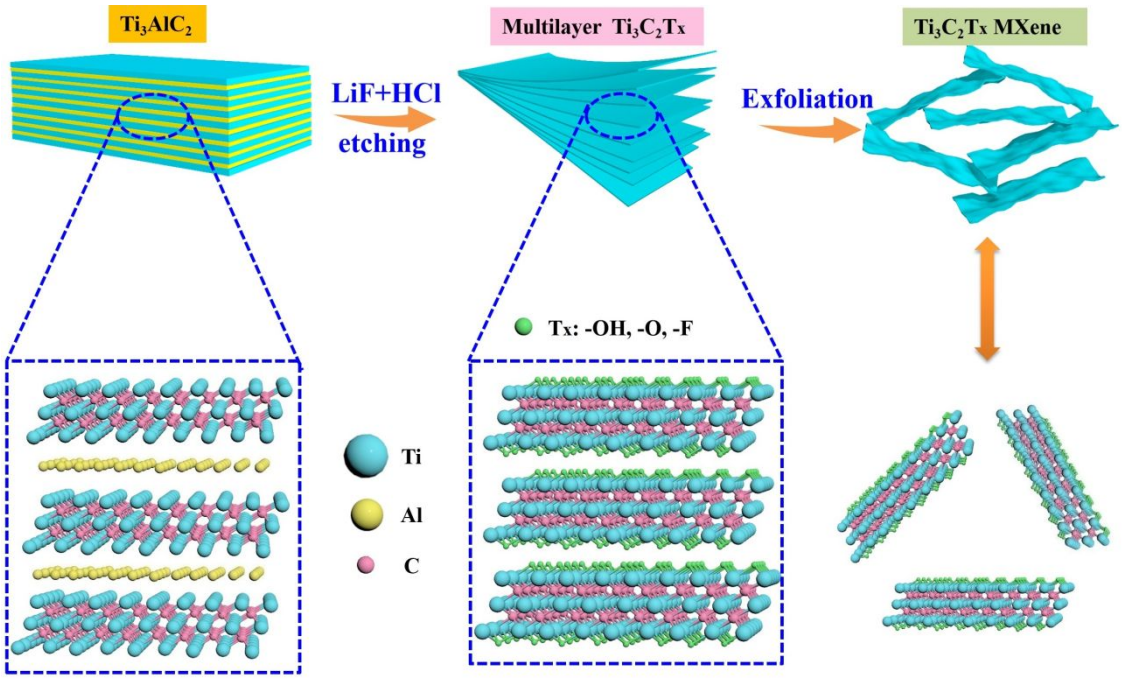

Figure S1. Illustration of synthesis of the $Ti_3C_2T_x$ MXene nanosheets.

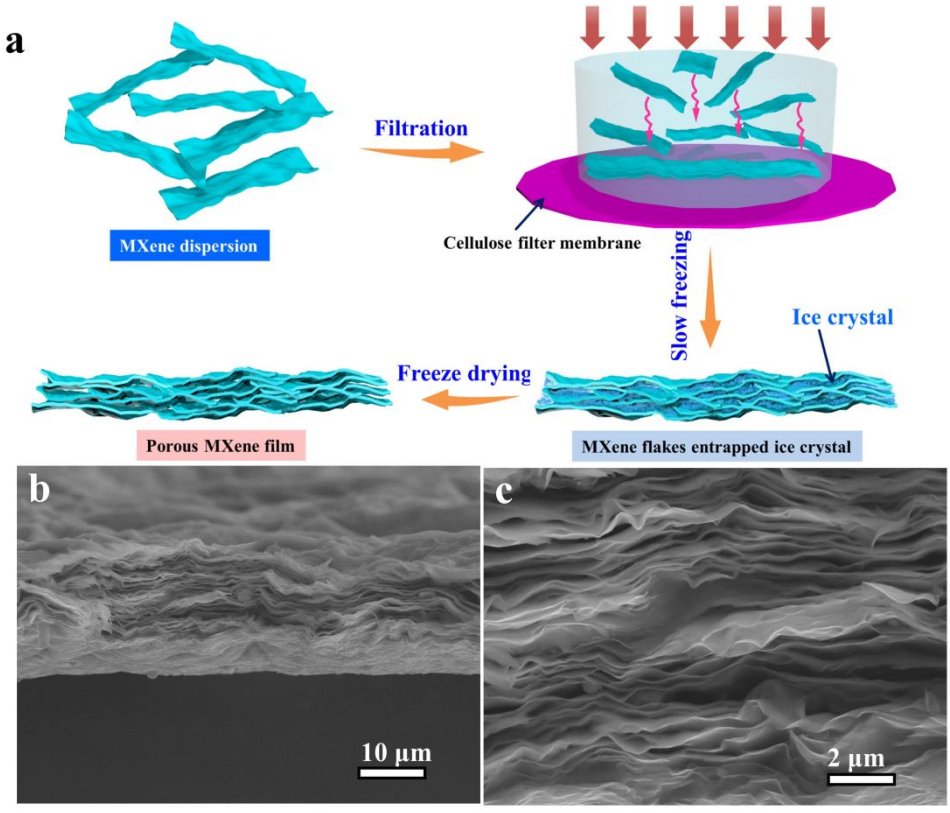

Figure S2. a) Illustration of synthesis of the porous MXene film using MXene dispersion (Main Steps: vacuum filtration; slow freezing; freeze drying), and b, c) the corresponding cross-sectional SEM images.

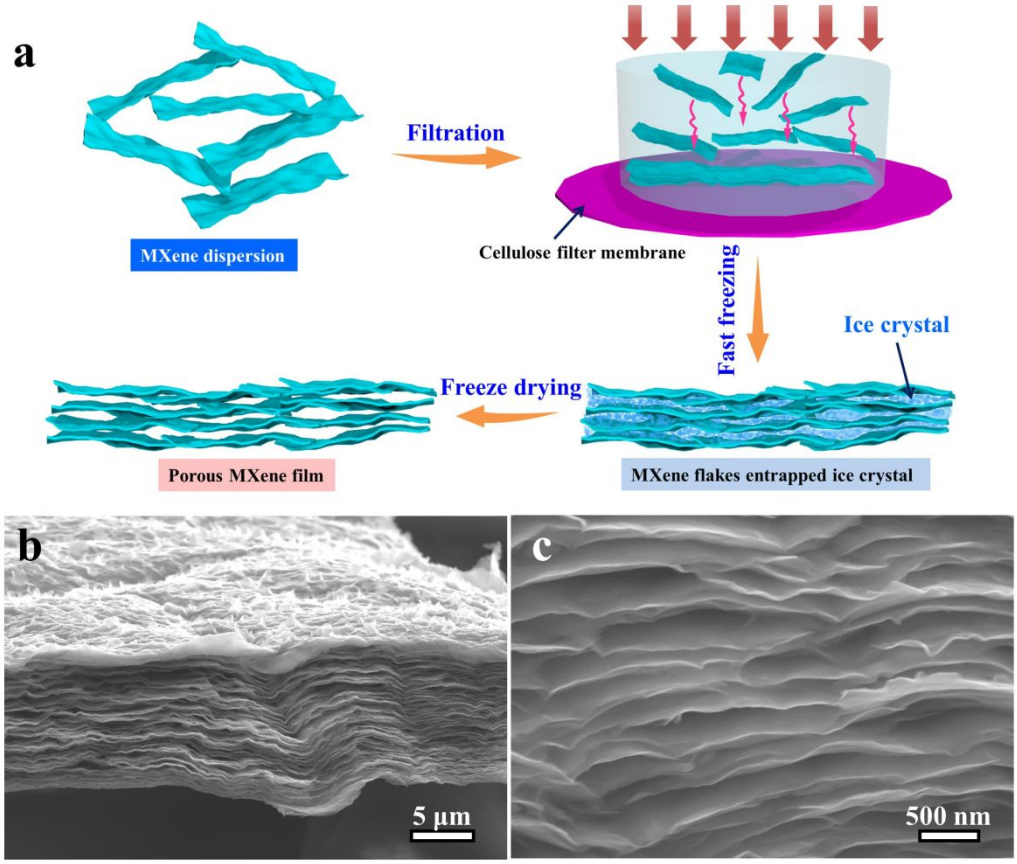

Figure S3. a) Illustration of synthesis of the porous MXene film using MXene dispersion (Main Steps: vacuum filtration; fast freezing; freeze drying), and b, c) the corresponding cross-sectional SEM images.

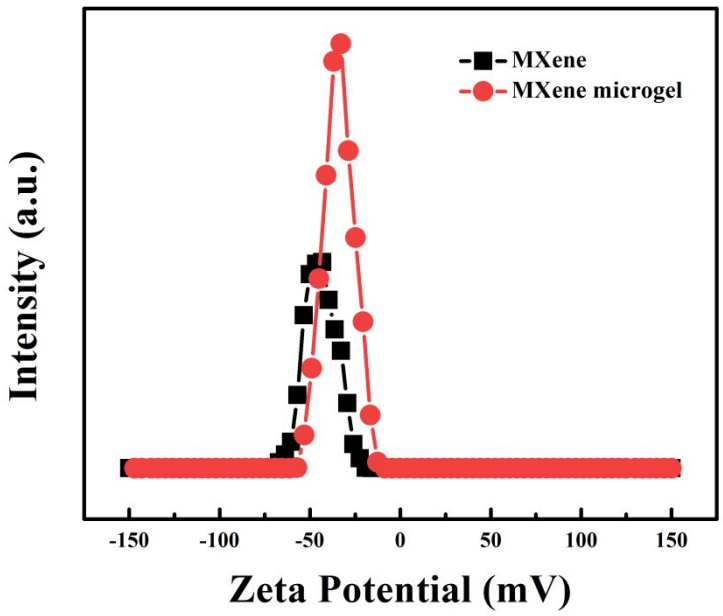

Figure S4. Zeta potential of MXene and MXene microgel.

Table S1. Comparison of filtration time between MXene film and 3D celluar MXene film.

Samples	Filtration time
MXene film	11160 s
3D $CMX_{0.1}$	941 s
3D $CMX_{0.2}$	290 s
3D $CMX_{0.5}$	35 s
3D $CMX_{1.0}$	26 s
3D $CMX_{2.0}$	18 s

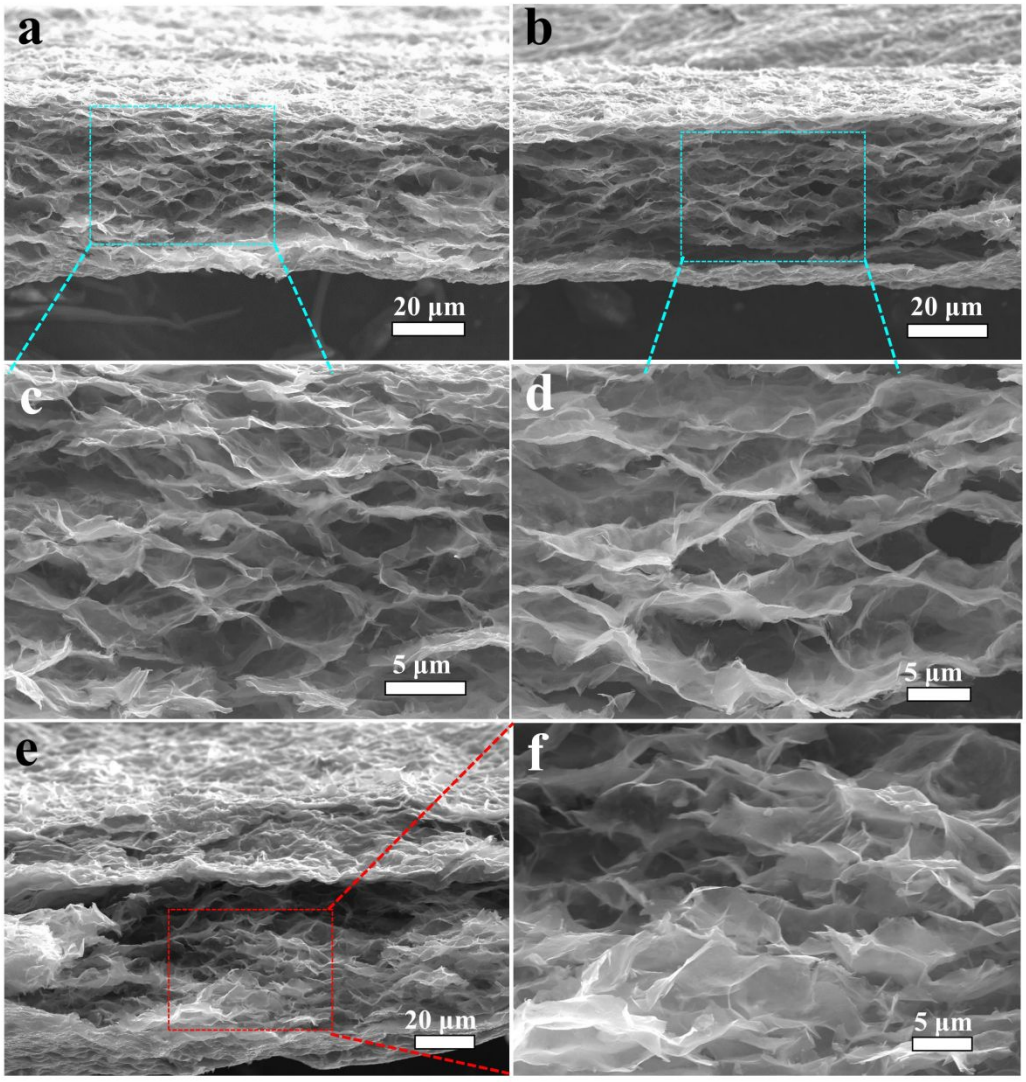

Figure S5. a-d) Cross-sectional SEM images of 3D celluar MXene film. e, f) Internal plane images of 3D celluar MXene film.

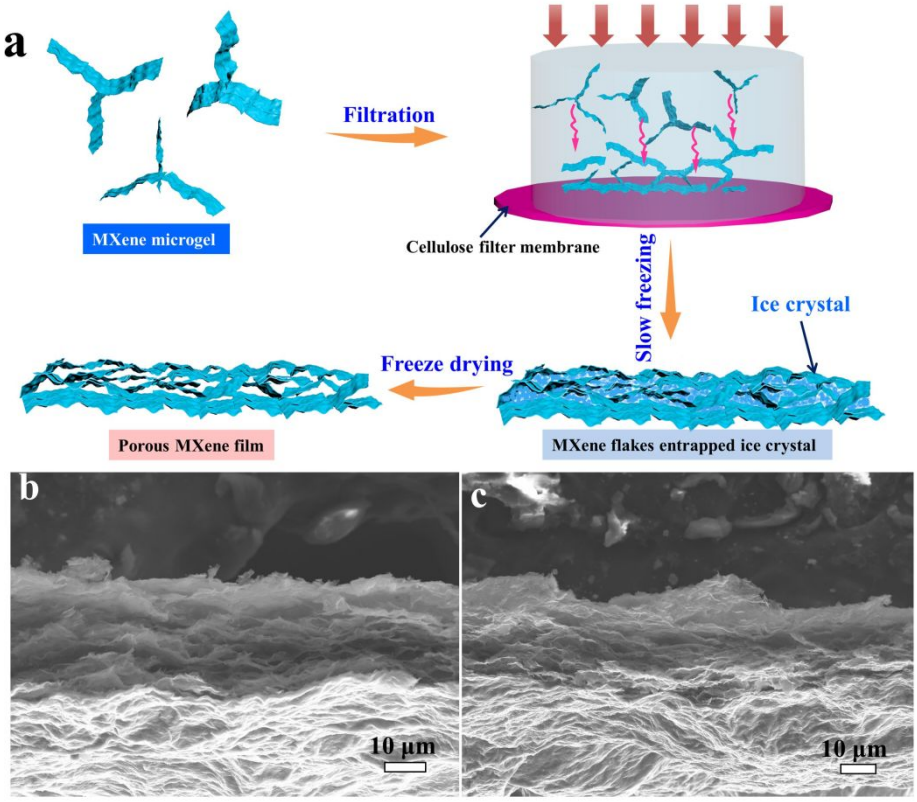

Figure S6. a) Illustration of synthesis of the porous MXene film using MXene microgel (Main Steps: vacuum filtration; slow freezing; freeze drying), and b, c) the corresponding cross-sectional SEM images.

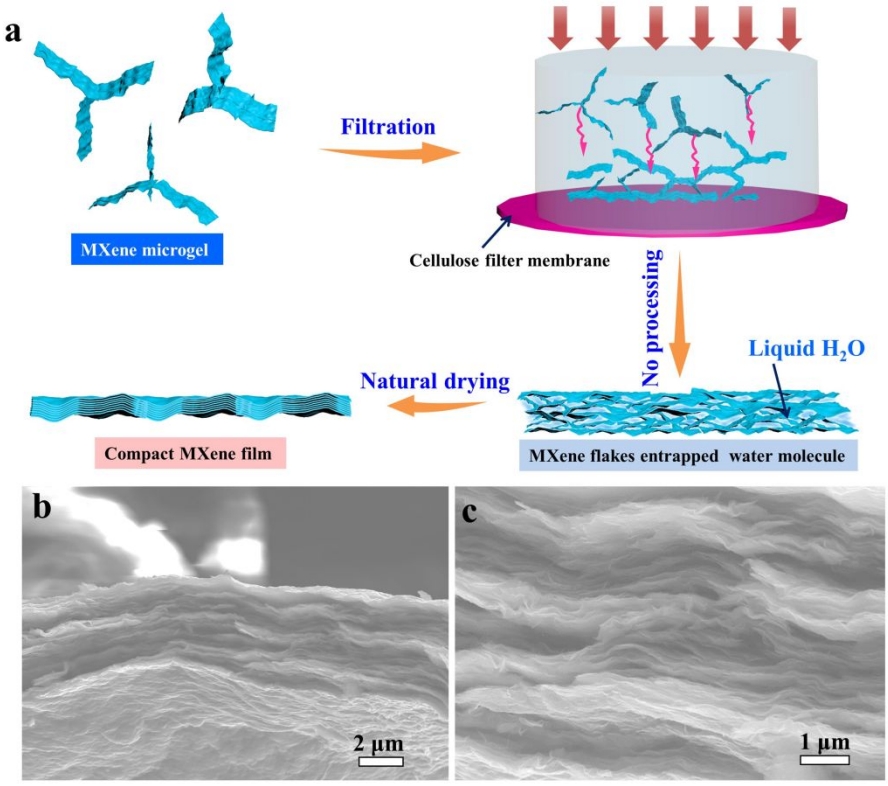

Figure S7. a) Illustration of synthesis of the compact MXene film using MXene microgel (Main Steps: vacuum filtration; no processing; natural drying), and b, c) the corresponding cross-sectional SEM images.

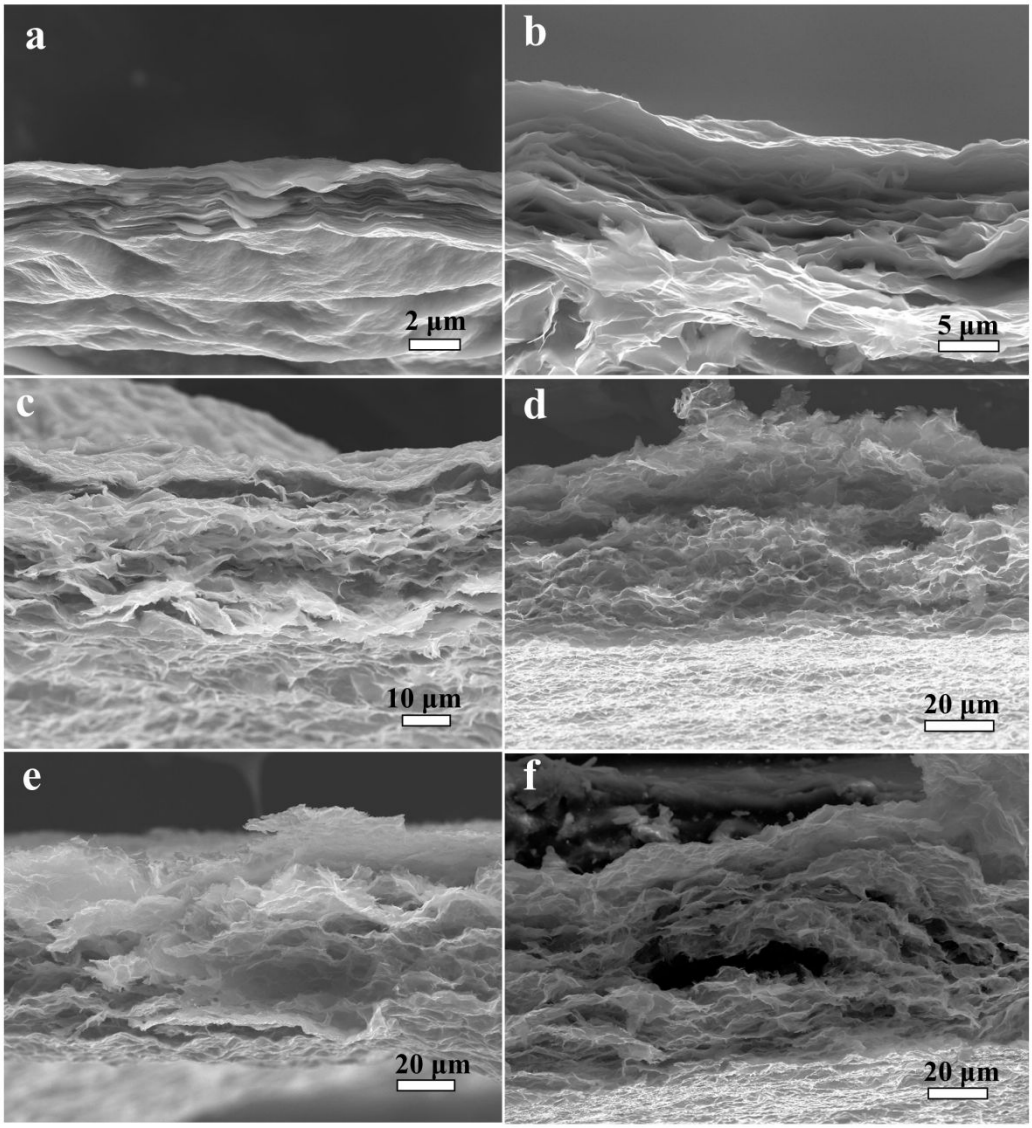

Figure S8. Cross-sectional SEM images of a) MXene film, b) 3D $CMX_{0.1}$, c) 3D $CMX_{0.2}$, d) 3D $CMX_{0.5}$, e) 3D $CMX_{1.0}$ and f) 3D $CMX_{2.0}$.

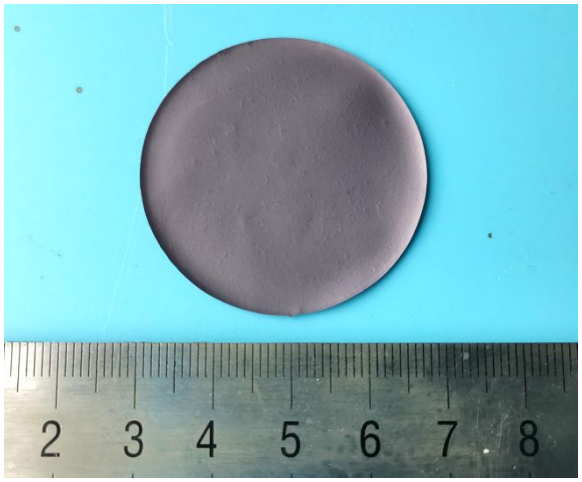

Figure S9. Digital photograph of MXene film.

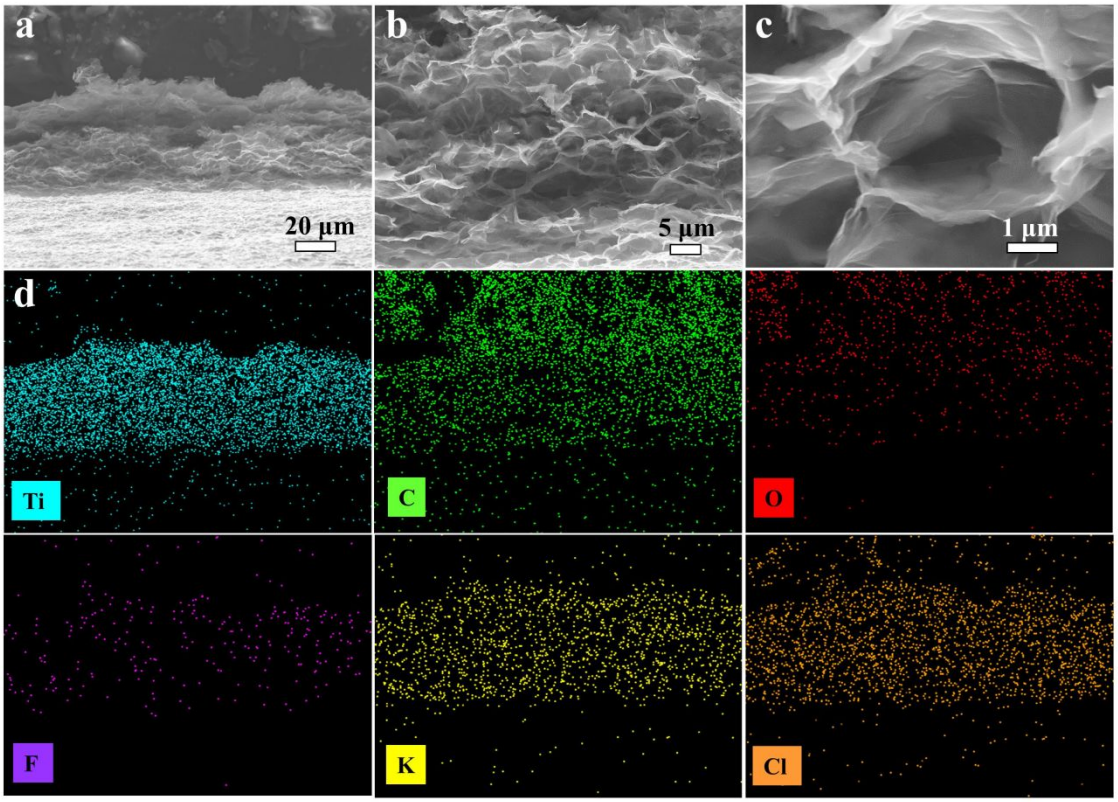

Figure S10. a-c) Cross-sectional SEM images of 3D $CMX_{0.5}$, and d) the corresponding EDX elemental mapping of Ti, C, O, F, K and Cl.

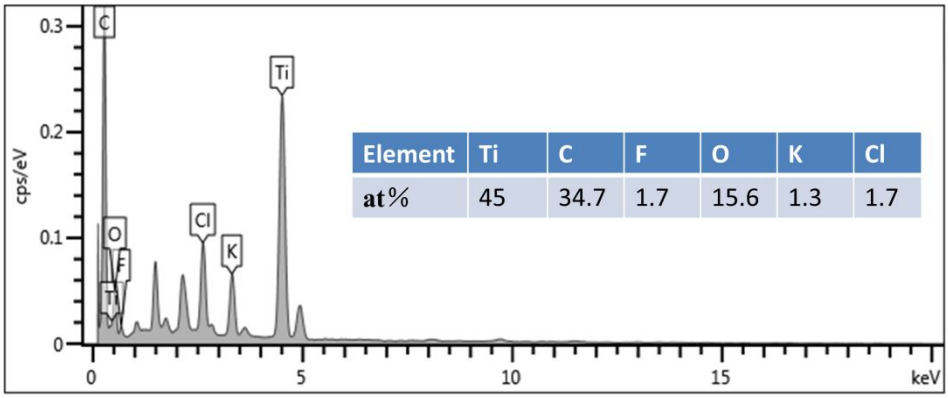

Element	Ti	C	F	O	K	Cl
at%	45	34.7	1.7	15.6	1.3	1.7

Figure S11. EDS result of 3D $CMX_{0.5}$.

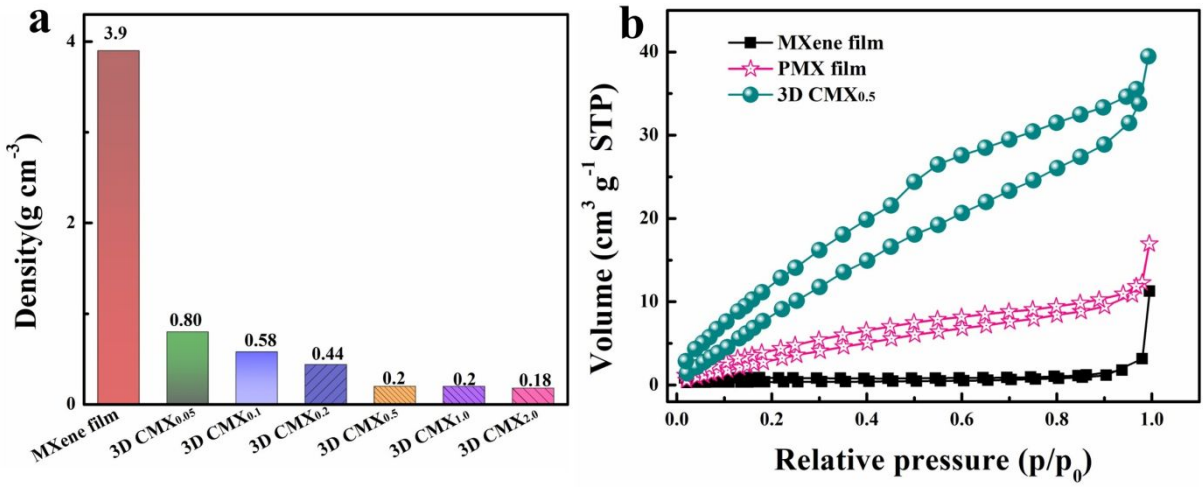

Figure S12. (a) The densities of the MXene film and 3D CMX. (b) N_2 adsorption−desorption isotherms of the MXene film, PMX film and 3D $CMX_{0.5}$.

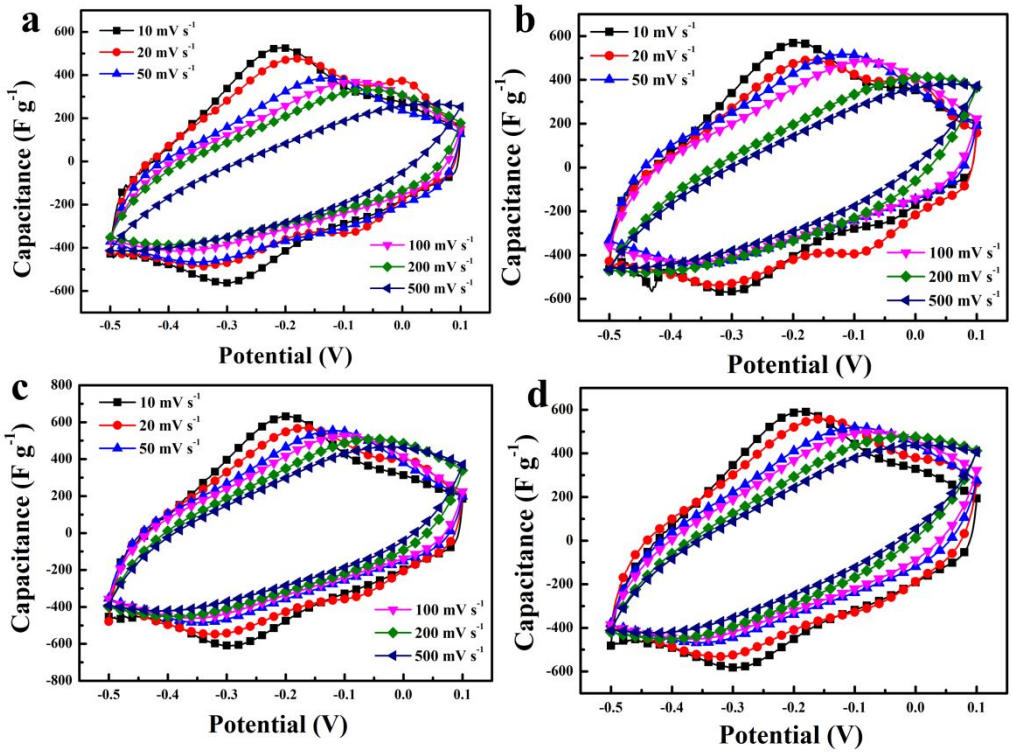

Figure S13. CV curves of a) 3D $CMX_{0.1}$, b) 3D $CMX_{0.2}$, c) 3D $CMX_{1.0}$ and d) 3D $CMX_{2.0}$ at the different scan rates ranging from 2 to 500 mV s^{-1}.

Table S2. Summary of capacitance of some electrodes

Electrode materials	Scan rate	C_g (F g^{-1})	Scan rate	C_g (F g^{-1})	Refs
Nanoporous MXene film	0.5 A g^{-1}	346	20 A g^{-1}	250.8	[1]
MXene/RGO	1 A g^{-1}	154.3	5 A g^{-1}	141.6	[2]
MXene/rGO	1 A g^{-1}	405	10 A g^{-1}	224.4	[3]
Multi-scaled MXene	1 A g^{-1}	372	20 A g^{-1}	193.4	[4]
Macroporous MXene	10 mV s^{-1}	310	—	—	[5]
MXene/ZnO	5 mV s^{-1}	120	100 mV s^{-1}	90	[6]
MXene/MnO_2	5 mV s^{-1}	130	200 mV s^{-1}	108	[7]
MXene	5 mV s^{-1}	118	200 mV s^{-1}	102.7	[8]
MXene/PPy	5 mV s^{-1}	416	100 mV s^{-1}	200	[9]
3D porous MXene/CNTs film	5 mV s^{-1}	375	1000 mV s^{-1}	251.2	[10]
Ultracompact MXene	2 mV s^{-1}	191.5	200 mV s^{-1}	96.7	[11]
MXene	2 mV s^{-1}	130	100 mV s^{-1}	80	[12]
MXene	2 mV s^{-1}	325	100 mV s^{-1}	137.5	[13]
MXene clay	2 mV s^{-1}	245	100 mV s^{-1}	204	[14]
MXene hydrogel	2 mV s^{-1}	380	—	—	[15]
3D MXene hydrogel	2 mV s^{-1}	272	1000 mV s^{-1}	226	[16]
MXene/rGO	2 mV s^{-1}	256	100 mV s^{-1}	193	[17]
MXene/rGO	2 mV s^{-1}	335.4	1000 mV s^{-1}	204	[18]
MXene/rHGO	2 mV s^{-1}	438	500 mV s^{-1}	302	[19]
3D Cellular MXene film	2 mV s^{-1}	**460**	500 mV s^{-1}	**324**	**This work**

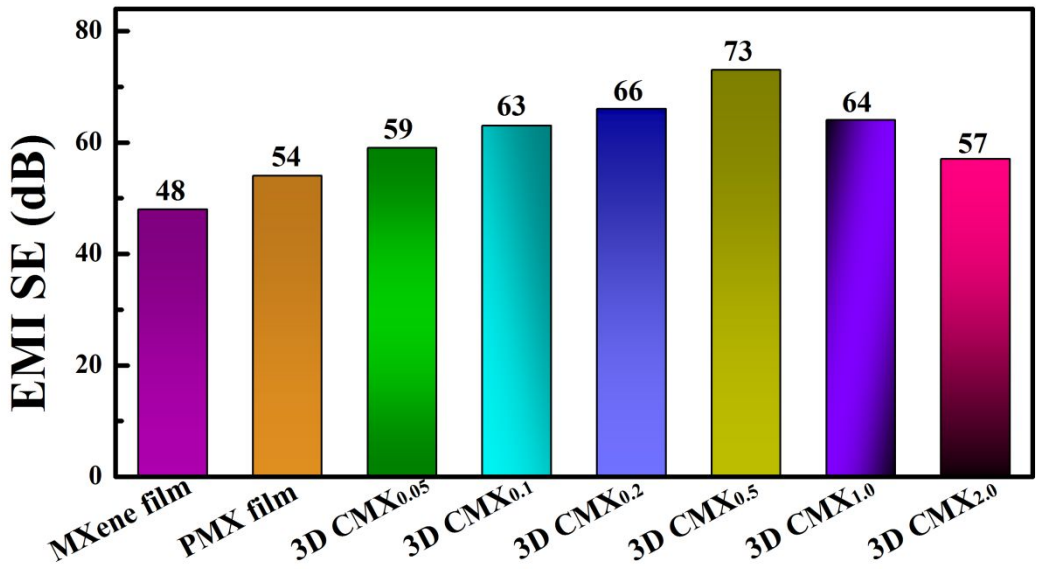

Figure S14. EMI SE values of the as-prepard samples with a mass of 15 mg at 8.2 GHz.

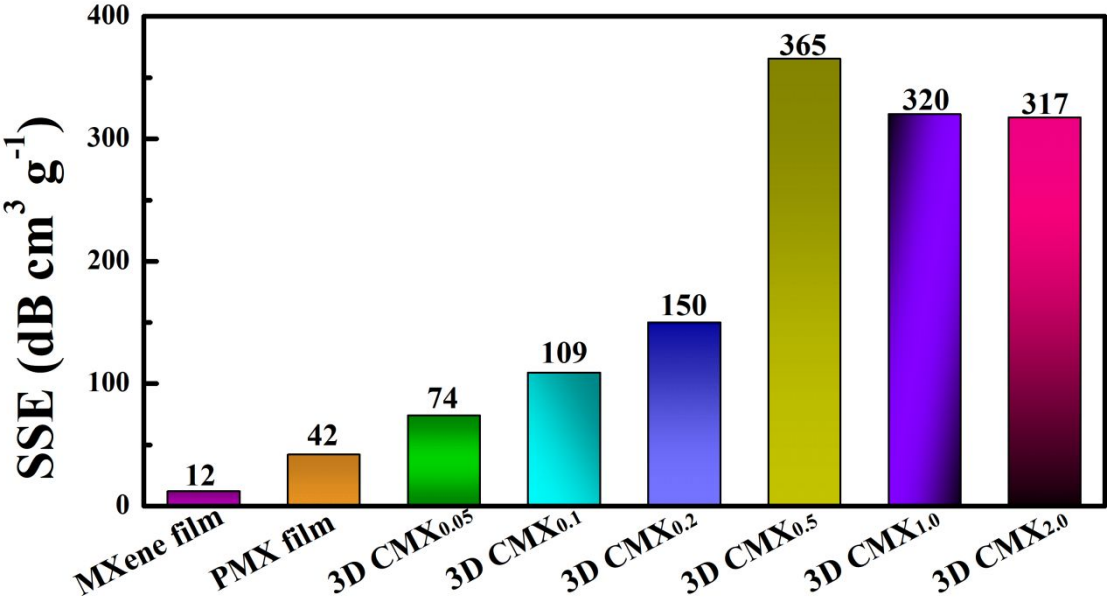

Figure S15. SSE values of the as-prepard samples with a mass of 15 mg at 8.2 GHz.

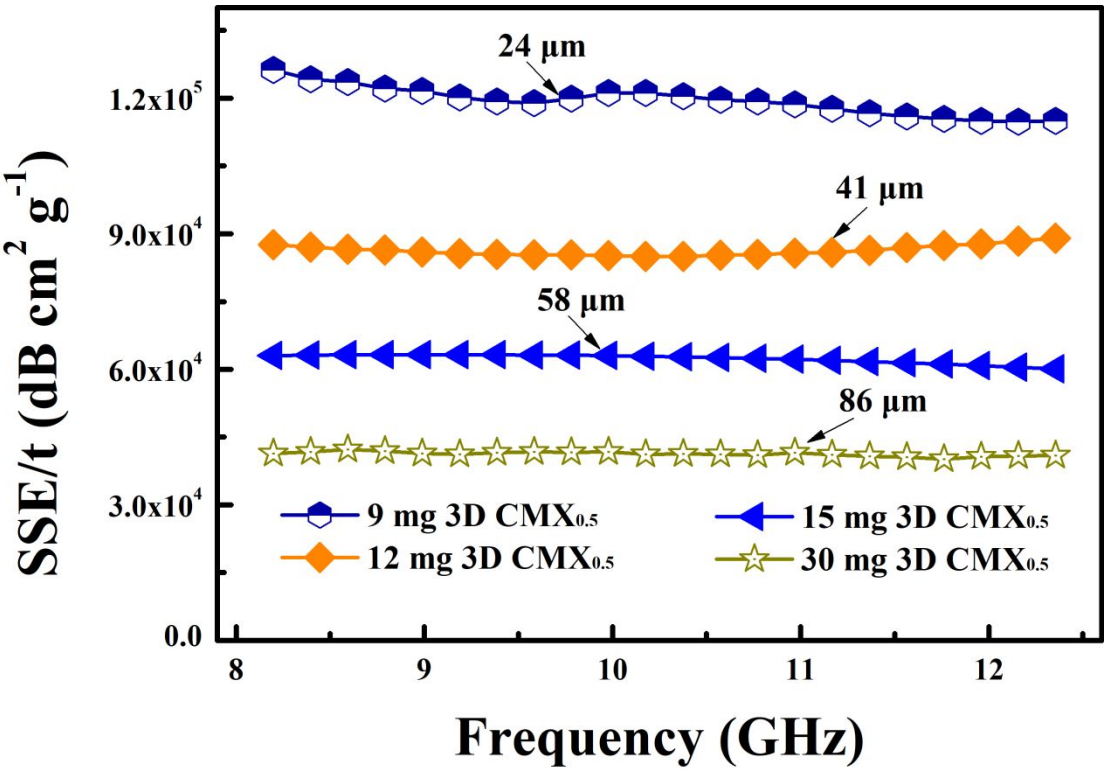

Figure S16. SSE/t values of the 3D $CMX_{0.5}$ with different thickness.

Table S3. Comparison of electromagnetic interference shielding performance for typical materials.

Materials	Thickness (mm)	EMI SE (dB)	SSE ($dB\ cm^3\ g^{-1}$)	SSE/t ($dB\ cm^2\ g^{-1}$)	Refs
Al foil	0.008	66	24.4	30555	[20]
Cu foil	0.01	70	7.8	7812	[20]
Carbon foam	2	40	241	1250	[21]
CNT-sponge	2.4	22	1100	4621	[22]
CNT-G foam	1.6	47	5280	33005	[23]
MWCNT-PS	2	30	57	285	[24]
MWCNT-PC	2.1	39	34.5	164	[25]
rGO	2.5	45.1	173	692	[26]
rGO-Fe_3O_4	0.3	24	31	1033	[27]
rGO-PEDOT	0.8	70	67.3	841	[28]
Graphene aerogel	3	37	529	1763	[29]
Graphene-PDMS	1	19.98	333	3330	[30]
Graphene foam	0.3	25.2	417	13889	[31]
MXene/CNFs	0.047	24	12	2647	[32]
MXene film	0.011	68	28.4	25863	[20]
MXene foam	0.018	50	125	69444	[33]
3D Cellular MXene film	**0.024**	**55**	**305**	**127083**	**This work**

References

(1) Fan, Z.; Wang, Y.; Xie, Z.; Xu, X.; Yuan, Y.; Cheng, Z.; Liu, Y. A Nanoporous MXene Film Enables Flexible Supercapacitors with High Energy Storage. *Nanoscale* **2018,** *10*, 9642–9652.

(2) Zhao, C.; Wang, Q.; Zhang, H.; Passerini, S.; Qian, X. Two-Dimensional Titanium Carbide/RGO Composite for High-Performance Supercapacitors. *ACS Appl. Mater. Interfaces* **2016,** *8*, 15661–15667.

(3) Xu, S.; Wei, G.; Li, J.; Han, W.; Gogotsi, Y. Flexible MXene-Graphene Electrodes with High Volumetric Capacitance for Integrated Co-Cathode Energy Conversion/Storage Devices. *J. Mater. Chem. A* **2017,** *5*, 17442–17451.

(4) Zhang, X.; Liu, Y.; Dong, S.; Yang, J.; Liu, X. Flexible Electrode Based on Multi-Scaled MXene ($Ti_3C_2T_x$) for Supercapacitors. *J. Alloy. Compd.* **2019,** *790*, 517–523.

(5) Lukatskaya, M. R.; Kota, S.; Lin, Z.; Zhao, M.-Q.; Shpigel, N.; Levi, M. D.; Halim, J.; Taberna, P.-L.; Barsoum, M. W.; Simon, P. Ultra-High-Rate Pseudocapacitive Energy Storage in Two-Dimensional Transition Metal Carbides. *Nat. Energy* **2017,** *2*, 17105.

(6) Wang, F.; Cao, M.; Qin, Y.; Zhu, J.; Wang, L.; Tang, Y. ZnO Nanoparticle-Decorated Two-Dimensional Titanium Carbide with Enhanced Supercapacitive Performance. *RSC Adv.* **2016,** *6*, 88934–88942.

(7) Tang, Y.; Zhu, J.; Yang, C.; Wang, F. Enhanced Supercapacitive Performance of Manganese Oxides Doped Two-Dimensional Titanium Carbide Nanocomposite in Alkaline Electrolyte. *J. Alloys Compd.* **2016,** *685*, 194–201.

(8) Zhu, J.; Tang, Y.; Yang, C.; Wang, F.; Cao, M. Composites of TiO_2 Nanoparticles Deposited on Ti_3C_2 MXene Nanosheets with Enhanced Electrochemical Performance. *J. Electrochem. Soc.* **2016,** *163*, A785–A791.

(9) Boota, M.; Anasori, B.; Voigt, C.; Zhao, M. Q.; Barsoum, M. W.; Gogotsi, Y. Pseudocapacitive Electrodes Produced by Oxidant-Free Polymerization of Pyrrole between the Layers of 2D Titanium Carbide (MXene). *Adv. Mater.* **2016,** *28*, 1517–1522.

(10) Zhang, P.; Zhu, Q.; Soomro, R. A.; He, S.; Sun, N.; Qiao, N.; Xu, B. In Situ Ice Template Approach to Fabricate 3D Flexible MXene Film-Based Electrode for High Performance Supercapacitors. *Adv. Funct. Mater.* **2020,** in press. DOI: 10.1002/adfm.202000922.

(11) Yang, C.; Tang, Y.; Tian, Y.; Luo, Y.; He, Y.; Yin, X.; Que, W. Achieving of Flexible, Free-Standing, Ultracompact Delaminated Titanium Carbide Films for High Volumetric Performance and Heat-Resistant Symmetric Supercapacitors. *Adv. Funct. Mater.* **2018,** *28*, 1705487.

(12) Lukatskaya, M. R.; Mashtalir, O.; Ren, C. E.; Dall'Agnese, Y.; Rozier, P.; Taberna, P. L.; Naguib, M.; Simon, P.; Barsoum, M. W.; Gogotsi, Y. Cation Intercalation and High Volumetric Capacitance of Two-Dimensional Titanium Carbide. *Science* **2013,** *341*, 1502–1505.

(13) Dall'Agnese, Y.; Lukatskaya, M. R.; Cook, K. M.; Taberna, P.-L.; Gogotsi, Y.; Simon, P. High Capacitance of Surface-Modified 2D Titanium Carbide in Acidic Electrolyte. *Electrochem. Commun.* **2014,** *48*, 118–122.

(14) Ghidiu, M.; Lukatskaya, M. R.; Zhao, M.-Q.; Gogotsi, Y.; Barsoum, M. W. Conductive Two-Dimensional Titanium Carbide 'Clay'with High Volumetric Capacitance. *Nature* **2014,** *516*, 78–81.

(15) Xia, Y.; Mathis, T. S.; Zhao, M.-Q.; Anasori, B.; Dang, A.; Zhou, Z.; Cho, H.; Gogotsi, Y.; Yang, S. Thickness-Independent Capacitance of Vertically Aligned Liquid-Crystalline MXenes. *Nature* **2018,** *557*, 409–412.

(16) Deng, Y.; Shang, T.; Wu, Z.; Tao, Y.; Luo, C.; Liang, J.; Han, D.; Lyu, R.; Qi, C.; Lv, W. Fast gelation of $Ti_3C_2T_x$ MXene Initiated by Metal Ions. *Adv. Mater.* **2019,** *31*, 1902432.

(17) Navarro-Suárez, A. M.; Maleski, K.; Makaryan, T.; Yan, J.; Anasori, B.; Gogotsi, Y. 2D Titanium Carbide/Reduced Graphene Oxide Heterostructures for Supercapacitor Applications. *Batteries Supercaps* **2018,** *1*, 33–38.

(18) Yan, J.; Ren, C. E.; Maleski, K.; Hatter, C. B.; Anasori, B.; Urbankowski, P.; Sarycheva, A.; Gogotsi, Y. Flexible MXene/Graphene Films for Ultrafast Supercapacitors with Outstanding Volumetric Capacitance. *Adv. Funct. Mater.* **2017,** *27*, 1701264.

(19) Fan, Z.; Wang, Y.; Xie, Z.; Wang, D.; Yuan, Y.; Kang, H.; Su, B.; Cheng, Z.; Liu, Y. Modified MXene/Holey Graphene Films for Advanced Supercapacitor Electrodes with Superior Energy Storage. *Adv. Sci.* **2018,** *5*, 1800750.

(20) Shahzad, F.; Alhabeb, M.; Hatter, C. B.; Anasori, B.; Hong, S. M.; Koo, C. M.; Gogotsi, Y. Electromagnetic Interference Shielding with 2D Transition Metal Carbides (MXenes). *Science* **2016,** *353*, 1137–1140.

(21) Moglie, F.; Micheli, D.; Laurenzi, S.; Marchetti, M.; Primiani, V. M. Electromagnetic Shielding Performance of Carbon Foams. *Carbon* **2012,** *50*, 1972–1980.

(22) Crespo, M.; González, M.; Elías, A. L.; Pulickal Rajukumar, L.; Baselga, J.; Terrones, M.; Pozuelo, J. Ultra-Light Carbon Nanotube Sponge as An Efficient Electromagnetic Shielding Material in the GHz Range. *Phys. Status Solidi–R* **2014,** *8*, 698–704.

(23) Song, Q.; Ye, F.; Yin, X.; Li, W.; Li, H.; Liu, Y.; Li, K.; Xie, K.; Li, X.; Fu, Q. Carbon Nanotube-Multilayered Graphene Edge Plane Core-Shell Hybrid Foams for Ultrahigh-Performance Electromagnetic-Interference Shielding. *Adv. Mater.* **2017,** *29*, 1701583.

(24) Arjmand, M.; Apperley, T.; Okoniewski, M.; Sundararaj, U. Comparative Study of Electromagnetic Interference Shielding Properties of Injection Molded Versus Compression Molded Multi-Walled Carbon Nanotube/Polystyrene Composites. *Carbon* **2012,** *50*, 5126–5134.

(25) Pande, S.; Chaudhary, A.; Patel, D.; Singh, B. P.; Mathur, R. B. Mechanical and Electrical Properties of Multiwall Carbon Nanotube/Polycarbonate Composites for Electrostatic Discharge and Electromagnetic Interference Shielding Applications. *RSC Adv.* **2014,** *4*, 13839–13849.

(26) Yan, D. X.; Pang, H.; Li, B.; Vajtai, R.; Xu, L.; Ren, P. G.; Wang, J. H.; Li, Z. M. Structured Reduced Graphene Oxide/Polymer Composites for Ultra-Efficient Electromagnetic Interference Shielding. *Adv. Funct. Mater.* **2015,** *25*, 559–566.

(27) Song, W.-L.; Guan, X.-T.; Fan, L.-Z.; Cao, W.-Q.; Wang, C.-Y.; Zhao, Q.-L.; Cao, M.-S. Magnetic and Conductive Graphene Papers toward Thin Layers of Effective Electromagnetic Shielding. *J. Mater. Chem. A* **2015,** *3*, 2097–2107.

(28) Agnihotri, N.; Chakrabarti, K.; De, A. Highly Efficient Electromagnetic Interference Shielding Using Graphite Nanoplatelet/Poly (3, 4-ethylenedioxythiophene)-poly (Styrenesulfonate) Composites with Enhanced Thermal Conductivity. *RSC Adv.* **2015,** *5*, 43765–43771.

(29) Song, W.-L.; Guan, X.-T.; Fan, L.-Z.; Cao, W.-Q.; Wang, C.-Y.; Cao, M.-S. Tuning Three-Dimensional Textures with Graphene Aerogels for Ultra-Light Flexible Graphene/Texture Composites of Effective Electromagnetic Shielding. *Carbon* **2015,** *93*, 151–160.

(30) Chen, Z.; Xu, C.; Ma, C.; Ren, W.; Cheng, H. M. Lightweight and Flexible Graphene Foam Composites for High-Performance Electromagnetic Interference Shielding. *Adv. Mater.* **2013,** *25*, 1296–1300.

(31) Shen, B.; Li, Y.; Yi, D.; Zhai, W.; Wei, X.; Zheng, W. Microcellular Graphene Foam for Improved Broadband Electromagnetic Interference Shielding. *Carbon* **2016,** *102*, 154–160.
(32) Cao, W.-T.; Chen, F.-F.; Zhu, Y.-J.; Zhang, Y.-G.; Jiang, Y.-Y.; Ma, M.-G.; Chen, F. Binary Strengthening and Toughening of MXene/Cellulose Nanofiber Composite Paper with Nacre-Inspired Structure and Superior Electromagnetic Interference Shielding Properties. *ACS Nano* **2018,** *12*, 4583–4593.
(33) Liu, J.; Zhang, H. B.; Sun, R.; Liu, Y.; Liu, Z.; Zhou, A.; Yu, Z. Z. Hydrophobic, Flexible, and Lightweight MXene Foams for High-Performance Electromagnetic-Interference Shielding. *Adv. Mater.* **2017,** *29*, 1702367.